Comprehensive Analytics for Reliability Evaluation of Conventional Isolated Multiswitch PWM DC–DC Converters

Hadi Tarzamni, *Student Member, IEEE*, Farhad Panahandeh Esmaeelnia, Mahmud Fotuhi-Firuzabad, *Fellow, IEEE*, Farzad Tahami, *Senior Member, IEEE*, Sajjad Tohidi, and Payman Dehghanian, *Member, IEEE*

***Abstract*—This article offers a holistic model and approach on reliability assessment of conventional isolated multiswitch pulsewidth modulation dc–dc (IMSDC-DC) power electronic converters with conventional half-bridge, full-bridge, and push-pull dc–dc topologies. The proposed reliability assessment analytics encapsulate correlated effects of several conditions (e.g., open- and short-circuit faults) and prevailing parameters (e.g., duty cycle, input voltage, output power, transformer turns ratio, voltage gain, switching frequency, operation time duration, and components characteristics) on the overall reliability performance of IMSDC-DC converters. Such insights are then harnessed within a Markov process to characterize and evaluate the mean time to failure reliability metrics for IMSDC-DC in both continuous and discontinuous conduction modes. Numerical results are followed with experimental verifications to demonstrate the self-embedded fault-tolerant capability of the IMSDC-DC topologies.**

***Index Terms*—DC–DC converters, Markov process, mean time to failure (MTTF), pulsewidth modulation (PWM), reliability.**

I. Introduction

With the rapid proliferation and the growingly dominant roles of modern power electronic converters in a wide range of mission-critical and high-cost applications, continuous assessment and monitoring of their reliability characteristics over time is very critical to ensure an acceptable functionality of the individual components as well as the systems they belong to [1]–[3]. Such analysis can be translated into meaningful information, which, in turn, offers constructive technical and economic instructions for informed decisions on best selecting, designing, and deploying different converters with appropriate configurations in various applications as the needs unfold [4], [5].

Various analytical frameworks for reliability analysis of power electronic converters, in general, and dc–dc converters, in particular, have been proposed. The emphasis on dc–dc converters is primarily driven by their widespread applications in renewable energy systems, electrical vehicles, aircraft, and home appliances [6]. Reliability-driven maintenance management of conventional boost converter is focused in [7], where the effects of characteristic changes in each element on the operating points of other components and the system's overall reliability profile are characterized and evaluated. It was concluded in [7] that the increase in the modeled series resistance of the main switch or the output capacitor would result in degradation of the converter's overall reliability performance. In [8], the *LC* filter in the conventional buck converter is designed where several critical factors, e.g., reliability, voltage and current ripples, power density, and cost are co-optimized. Furthermore, the relationship between the filter capacitor lifetime and its electro-thermal stress is characterized with keen considerations to values and types of the filter capacitance and inductance. In [9], reliability of a three-phase soft-switching interleaved boost converter is evaluated and compared to hard switching interleaved boost converter and the interleaved configuration in [10] and [11]. With the main goal to achieve a cost-effective operational design with an optimal number of interleaved boost converters, reliability of a pulsewidth modulation (PWM) boost converter in interleaved operating modes (where all parallel converters are operating) vs. a semiredundant operating condition (where one converter operates while the others are in standby) is analyzed in [12]. In [13], Markov models are utilized to evaluate the reliability of single-stage and interleaved conventional boost converters. It was concluded that a two-stage interleaved boost converter with half power operation of one stage after the failure of the other offers higher reliability than that in a conventional single-stage boost converter. In [14], reliability of the multiphase dc–dc converters in photovoltaic energy conversion systems is evaluated, where a tradeoff is achieved between the capacitor voltage ripples and the converter reliability by selecting an optimal set of capacitors. In [15], reliability of a full soft-switching boost converter is compared with its interleaved topology and

Manuscript received December 27, 2018; revised May 31, 2019; accepted September 16, 2019. Date of publication September 30, 2019; date of current version February 11, 2020. Recommended for publication by Associate Editor F. H. Khan. *(Corresponding author: Farzad Tahami.)*

H. Tarzamni, M. Fotuhi-Firuzabad, and F. Tahami are with the Department of Electrical Engineering, Sharif University of Technology, Tehran 11365/8639, Iran (e-mail: hadi_tarzamni@ee.sharif.edu; fotuhi@sharif.edu; tahami@sharif.edu).

F. P. Esmaeelnia and S. Tohidi are with the Faculty of Electrical and Computer Engineering, University of Tabriz, Tabriz 5166616471, Iran (e-mail: farhadpanahandeh@gmail.com; stohidi@tabrizu.ac.ir).

P. Dehghanian is with the Department of Electrical and Computer Engineering, George Washington University, Washington, DC 20052 USA (e-mail: payman@gwu.edu).

Color versions of one or more of the figures in this article are available online at http://ieeexplore.ieee.org.

Digital Object Identifier 10.1109/TPEL.2019.2944924

hard switching conventional PWM boost converter, where it reveals that the interleaved soft-switching two-phase converter is attributed a higher reliability performance. In [16], a four-step fault-tolerant full-bridge (FB) dc–dc converter design with phase shift control is presented and its fault-tolerant capability and enhanced reliability under open circuit (OC) fault conditions are analyzed. In particular, the main goal in [16] is to diagnose and tolerate different component failures, where the fault diagnosis is performed through one additional winding to the primary side of the transformer: if an OC fault occurs in any primary-side switch, the fault detection module operates and the control system triggers an active phase shift to tolerate the fault.

Fault tolerance is found to be a prevalent issue in improving the reliability of power electronic converters [17], [18], which facilitates a continuous operation during faults. Majority of techniques to realize a higher fault tolerance capability—i.e., a durable power transfer to the output load during fault scenarios—are centered on utilizing hardware and software reconfigurations. In dc–ac converters, extra power electronic components along with the fault detection systems are commonly integrated to help the inverter continue its function in a de-rated operating state [19]–[22]. For instance, several extra switches and additional number of relays are utilized in [19] to engender a fault tolerance capability. This procedure is somehow approached in dc–dc converters too, where interleaving aids a heightened fault tolerance [9], [10], [13], [15]: extra components with the same configuration as the main converter are added that can help an acceptable converter functionality when a failure occurs.

In almost all previous efforts on fault-tolerant converter design and analysis, external components, fault detection elements, input current sharing techniques, and complicated control systems are required. However, conventional isolated FB, half-bridge (HB), and push-pull (PP) dc–dc topologies are driven by several operational characteristics that, if harnessed meticulously, can help in fault tolerance realization with no additional power electronic components nor complicated control algorithms. Such a self-embedded fault-tolerant capability is addressed in this article, where the focus is on reliability analyses of conventional isolated multiswitch PWM DC-DC (IMSDC-DC) converters with FB, HB, and PP DC–DC topologies. Different from the existing literature, where the dc–dc converter reliability is solely driven by parameters including time durations and some particular characteristics of the elements [14], [16], this article offers comprehensive analytics for reliability assessment of IMSDC-DC converters that well capture:

1) the effects of different parameters [e.g., duty cycle (D), input voltage (V_i), output power (P_o), transformer turn ratio (n), voltage gain (G), switching frequency (f_s), components characteristics, and operational time durations (t)];
2) different conditions under short circuit (SC) and OC faults of the converter components;
3) different operating modes of the converter [i.e., continuous and discontinuous conduction modes (CCM and DCM)].

The sensitivity of the components failure rates within a converter are presented with respect to each of the above parameters and the mean time to failure (MTTF) metric of reliability is assessed as a determinative operational factor for IMSDC-DC converters, altogether verifying the self-embedded fault-tolerant capability of IMSDC-DC converters under OC fault scenarios.

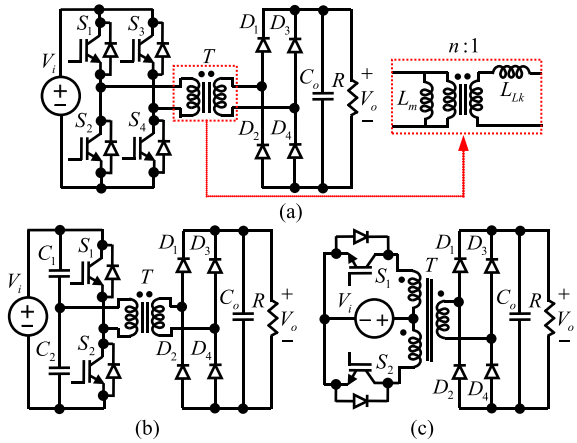

Fig. 1. IMSDC-DC converters. (a) FB. (b) HB. (c) PP.

II. Operation Principles of IMSDC-DC Converters

In this section, the main principles of a self-embedded fault-tolerant IMSDC-DC converter under OC faults of its components are presented. The basic topologies of IMSDC-DC converters are presented in Fig. 1, where the nonideal transformer is modeled via an ideal transformer with a turns ratio of n : 1 along with magnetizing (L_m) and leakage (L_{Lk}) inductances. According to the self-embedded fault-tolerant capability of the IMSDC-DC converters, three main operational conditions can be realized as follows.

A. Full Power Operating State (Healthy State)

In this operating state, all converter components are in their healthy operating condition and the converter operates in its full power capacity: the semiconductors voltage stresses are low as prescribed by their design specifications; the transformer is utilized in its optimal operation reflected by its core bipolar operation—bipolar operation is commonly perceived in IMSDC-DC converters since their transformer core primary winding is driven by both positive and negative voltage levels, and, therefore, the core is designed in smaller sizes and utilized more efficiently [23].

B. Partial Power Operating Sate (De-Rated States)

In such operating states, one or several components within the converter faces OC faults and the converter can continue functioning in a de-rated operation capacity, i.e., the output power decreases and the stresses on the converter components increase compared to that of the full power operation. In such circumstances, the converter does not encounter a full output power cut, making it still possible to serve the nonsensitive loads. The de-rated operating states of an HB converter are depicted in Fig. 2.

As illustrated in Fig. 2(a), the S_1 switch faces an OC fault and the converter de-rated functionality appears similar to that of the flyback converter. In such a scenario, half of the converter

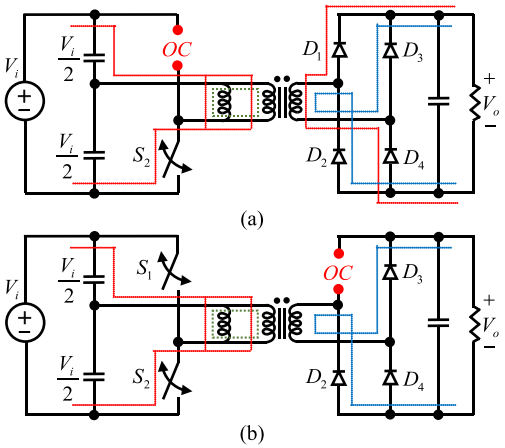

Fig. 2. De-rated operating states of an HB converter under OC scenarios. (a) OC of S_1. (b) OC of D_1.

switching period—originally operated by this switch—becomes inactive, while the HB converter can continue its power transfer to the output load in the other half switching period, operated by the S_2 switch. As noticed, such an operation mimics that of a flyback converter with an input blocking capacitor and two series secondary-side diodes. Unlike the healthy HB states, L_m stores magnetic energy and transfers this energy to the output load. Note that the transformer core is primarily designed for the HB bipolar operation, while in such operating states, the flyback operation is driven by a unipolar core utilization. However, the designed core is suitable for the de-rated power density in the flyback operation. On the other hand, $L_{\rm Lk}$ can be negligible in this operation since the design requirements of HB converters necessitate much higher L_m values than $L_{\rm Lk}$.

In Fig. 2(b), the D_1 diode faces an OC fault, resulting in a de-rated operating state of the converter; L_m is charged through the input blocking capacitor and theS_2 switch with $V_i/2$. When S_2 is turned OFF, the stored energy is transferred to the output load through D_2 and D_3 similar to the process in the flyback converter. As noted earlier, the converter has a self-embedded fault-tolerant capability in response to some OC fault incidents, which is satisfied with no additional auxiliary hardware or software component requirements. The OC faults under which the IMSDC-DC converters operate in a de-rated (partial power) operating state are listed as follows.

1) OC faults on one of the primary (secondary)-side switches (diodes), or simultaneous incidents on corresponding switches (diodes), e.g., OC faults on S_1 and S_4 switches, or D_1 and D_4 diodes.
2) OC faults on one of the input blocking capacitors in the HB converter.
3) Simultaneous OC faults on corresponding switches and diodes from the primary and secondary sides, e.g., OC faults on S_1 and D_1 in the FB converter.

C. Total Failure Operating State (Absorbing State)

This operating state reflects a total failure of the converter with no power transfer ability to the output load. The following is a list of conditions where a converter total failure is realized:

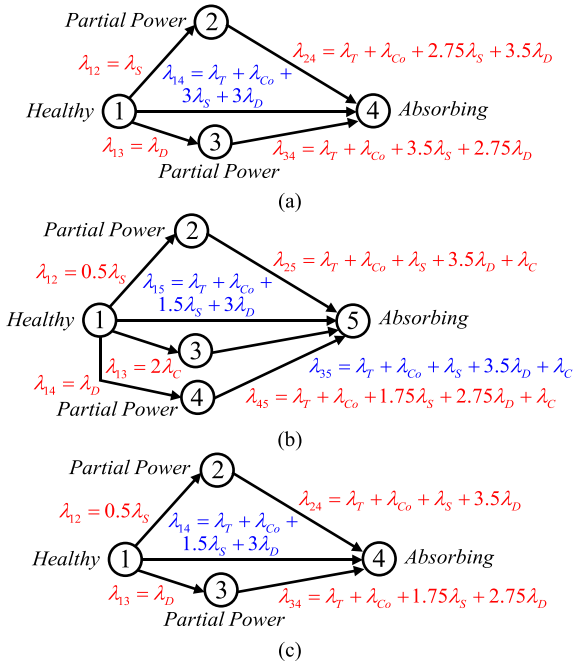

Fig. 3. Markov model of the IMSDC-DC converters. (a) FB. (b) HB. (c) PP.

1) SC fault in each component;
2) simultaneous OC faults on switches or diodes in one leg, e.g., OC faults on S_1 and S_2, or D_1 and D_2;
3) simultaneous faults in both input blocking capacitors of the HB converter;
4) simultaneous OC faults on complementary switches or diodes in one side, e.g., OC faults on D_1 and D_3;
5) simultaneous OC faults on complementary switches and diodes from the primary and secondary sides, e.g., OC faults on S_1 and D_3 in the FB converter.

III. Markov Model

Continuous Markov process is commonly approached to probabilistically model and solve large-scale problems in various disciplines. In this article, Markov process is employed to model and formulate the reliability characteristics and performance of IMSDC-DC converters. Built on the discussions on the OC and SC fault scenarios and the corresponding IMSDC-DC operating states (see Section II), the suggested Markov models for the IMSDC-DC converters are illustrated in Fig. 3, where the FB, HB, and PP dc–dc converters are attributed four, five, and four operating states in their Markov models, respectively. The first and the last states are designated as the healthy and absorbing states, respectively, and the other intermediate states reflect the de-rated operating states (states 2 and 3 for FB and PP converters, and states 2, 3, and 4 for HB converter). Note that, the proposed models in Fig. 3 are accurate for all bridge-type dc–dc converters.

According to the suggested Markov models in Fig. 3, the reliability of an IMSDC-DC converter is evaluated as follows:

$$R(t)=\sum_{i=1}^{s}P_i(t) \tag{1}$$

where $P_i(t)$ is the probability of operating state i and s is the total number of healthy and de-rated operating states—i.e., s is equal to three, four, and three for FB, HB, and PP converters, respectively. Note that $R(t)$ is equal to $P_1(t)$ for sensitive loads that could not tolerate the de-rated operating states of the converters. In order to evaluate $P_i(t)$, a state-space matrix equation is characterized as follows:

$$d/dt\left[P_1(t)\cdots P_{s+1}(t)\right]=\left[P_1(t)\cdots P_{s+1}(t)\right]\times[\mathbf{A}] \tag{2}$$

where $[\mathbf{A}]$ is determined as

$$[\mathbf{A}]=\begin{cases}\begin{bmatrix}\lambda_{11}&\lambda_{12}&\lambda_{13}&\lambda_{14}\\0&\lambda_{22}&0&\lambda_{24}\\0&0&\lambda_{33}&\lambda_{34}\\0&0&0&0\end{bmatrix} & \text{for FB and PP converters}\\ \begin{bmatrix}\lambda_{11}&\lambda_{12}&\lambda_{13}&\lambda_{14}&\lambda_{15}\\0&\lambda_{22}&0&0&\lambda_{25}\\0&0&\lambda_{33}&0&\lambda_{35}\\0&0&0&\lambda_{44}&\lambda_{45}\\0&0&0&0&0\end{bmatrix} & \text{for HB converter}\end{cases} \tag{3}$$

and $\lambda_{ij}(i\neq j)$ is the failure rate of the converter from an operating state i to j, which indicates the occurrence of one fault in that transition. λ_{ii} is defined as the negative summation of other failure rates in row i in matrix $\mathbf{A}$, as all elements in each row of this matrix should sum up to zero [24]. λ_{ii} is only a mathematical concept that does not relate to any real fault occurrence. Practical observations reveal the fact that the SC faults are more probable to happen than the OC faults on power electronic semiconductor devices [25]. Accordingly, probabilities of 3/4 and 1/4 are assumed on a switch or diode that encounters SC and OC faults, respectively. Additionally, only SC faults are considered for passive components within IMSDC-DC converters which have been reflected in λ_{ij} in Fig. 3. For instance, λ_{34} for the FB converters in Fig. 3(a) is assessed as follows:

$$\begin{aligned}\lambda_{34}=\lambda_T+\lambda_{Co}+(2\times0.25\lambda_S)+(4\times0.75\lambda_S)\\+(2\times0.25\lambda_D)+(3\times0.75\lambda_D)\end{aligned} \tag{4}$$

where $\lambda_S,\lambda_D,\lambda_T,\lambda_C$, and λ_{Co} are, respectively, the failure rates corresponding to the switch, diode, transformer, input blocking, and output capacitor. The failure rates are primarily driven by several different factors such as quality, material, voltage stress, environmental conditions, temperature, power loss, etc., which are introduced and formulated in MIL-HDBK-217 [26], [27]. Note that, while constant in each operating state, the failure rate of each component varies in different states, since the power loss and stresses on each component dynamically change during transitions. Such an assumption is valid only when the component resides in its useful operating lifetime as prescribed in the component failure rate curve commonly referred as the bath-tub curve (see Fig. 4). As illustrated in Fig. 4, each component is attributed to three operating intervals in its lifetime, namely debugging, useful lifetime, and wear-out [24].

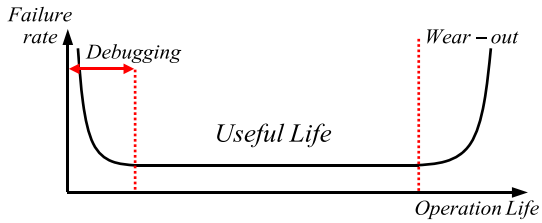

Fig. 4. Failure rate of a component in its operating lifetime [24].

Assuming the component's initial state as the healthy operating state, the initial condition in (2) is expressed as

$$\left[P_1(0)\quad P_2(0)\quad\cdots\quad P_{s+1}(0)\right]=\left[1\quad0\quad\cdots\quad0\right]. \tag{5}$$

Accordingly, $P_i(t)$ is calculated as

$$P_i(t)=\begin{cases}e^{\lambda_{ii}t}; & i=1\\ \frac{\lambda_{1i}}{\lambda_{11}-\lambda_{ii}}\left(e^{\lambda_{11}t}-e^{\lambda_{ii}t}\right); & i\neq1.\end{cases} \tag{6}$$

Eventually, the MTTF metric of reliability is defined as follows:

$$\text{MTTF}=\int_{t=0}^{\infty}R(t)dt=\frac{-1}{\lambda_{11}}+\sum_{i=2}^{s}\frac{\lambda_{1i}}{\lambda_{11}-\lambda_{ii}}\left(\frac{1}{\lambda_{ii}}-\frac{1}{\lambda_{11}}\right) \tag{7}$$

where $\lambda_{ii}(i=1,\ldots,s)$ and $\lambda_{1i}(i=2,\ldots,s)$ have negative and positive values, respectively.

IV. Reliability Assessments: Numerical Results

This section presents the reliability evaluation results of the three IMSDC-DC converters, considering variations in different prevailing parameters D, V_i, P_o, n, G, f_s, t, and components operational characteristics in both DCM and CCM operation modes. The reliability assessment of the converters is approached based on the steady state and power loss analytics provided in [23]. The IMSDC-DC converters components are designed with $L_m=5$ mH, $L_{Lk}=500$ μH, $C_1=C_2=C_o=33$ μF, and $R=100$ Ω. Minimum and maximum acceptable duty cycles are $D_{\min}=0.1$ and $D_{\max}=0.5$, since the complementary switches should be driven with nonoverlapping voltage pulses to prevent cross conduction of the switches in one leg [23]. Sample semiconductor devices are assumed for the switch and diode, where a forward ON voltage drop of 1 V and drain-source ON-resistance of 0.049 Ω are assumed for the switch and 1.5 V and 23 mΩ for the diode. Furthermore, passive components are considered nonideal. Sensitivity analysis to investigate the effects of variations in the aforementioned parameters is evaluated next. The initial values of $P_o=100$ W, $f_s=20$ kHz, $n=1$, $t=0.6\times10^6$ h, and DCM and CCM duty cycles of 1/6 and 1/3 are assumed, which will vary in the test case scenarios of assessing their own impacts on the overall reliability of converters. With the above assumptions, design and components characteristics, the IMSDC-DC reliability evaluations are as follows.

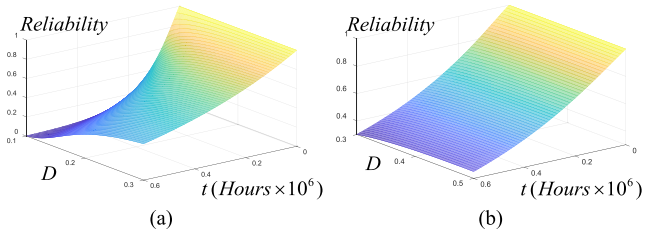

Fig. 5. Reliability performance with respect to duty cycle and time duration. (a) DCM HB. (b) CCM HB.

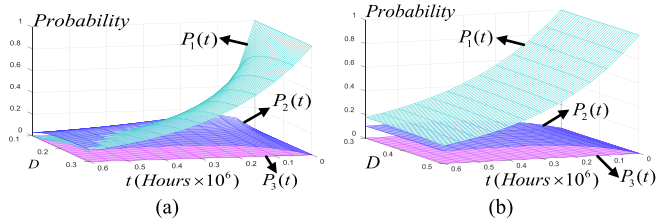

Fig. 6. Probability of operating states with respect to duty cycle and time duration. (a) DCM FB. (b) CCM FB.

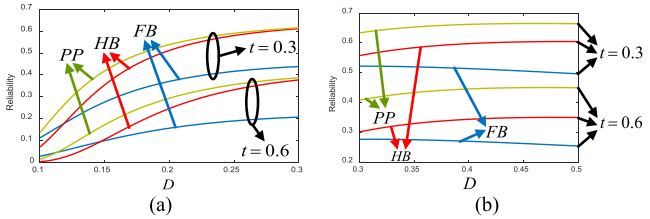

Fig. 7. Reliability comparison of IMSDC-DC converters with respect to duty cycle at $t = 0.3 \times 10^6$ and 0.6×10^6 h. (a) DCM operation. (b) CCM operation.

A. Duty Cycle

In this section, the reliability of the IMSDC-DC converters is assessed in DCM and CCM with variable parameters of D and t. With the initial assumptions described above and following the equations in Section III [23], [24], the boundary duty cycle between DCM and CCM is evaluated as $D_B = 0.3$. The components failure rates in a CCM HB converter for its healthy state are calculated as follows:

$$\lambda_S(D) = 0.48 \exp\left(-1925\left(\frac{1}{298+42.694D+\frac{2.116}{D^2}}-\frac{1}{298}\right)\right) \tag{8}$$

$$\lambda_D(D) = 0.0038 \times \left(\frac{1}{6D}\right)^{2.43} \times \exp\left(-3091\left(\frac{1}{355.968+0.736D}-\frac{1}{298}\right)\right) \tag{9}$$

$$\lambda_T(D) = 0.049\exp\left(-1276\left(\frac{1}{302.125+41.25D}-\frac{1}{298}\right)\right) \tag{10}$$

$$\lambda_C(D) = 7.63 \times 10^{-3}\left(2.37D^3+1\right) \tag{11}$$

$$\lambda_{Co}(D) = 1.154 \times 10^{-2} \tag{12}$$

in which the impact of D on $\lambda_{Co}(D)$ is negligible. With the suggested Markov model, three-dimensional plots representing the reliability of DCM and CCM HB converters with respect to the duty cycle and time durations are illustrated in Fig. 5. One can see, in Fig. 5(a) and (b), that the HB converter reliability enhances as the duty cycle increases in both DCM and CCM operations, and it reaches a maximum in $D = D_{\max}$. This reliability enhancement in higher D values is primarily due to the fact that the HB converter requires a lower input voltage to reach a constant output power as desired $(G = D/n)$. Consequently, the lower the input voltage, the lower the voltage stress on the components and the higher the overall reliability performance of the converter is. Moreover, reliability of the HB converter decreases over time due to aging and deterioration mechanisms which increase the component's failure probability. The operating state probabilities for an FB converter are assessed as demonstrated in Fig. 6. According to Fig. 6(a) and (b), $P_3(t)$ is attributed to the lowest probability in both DCM and CCM operation modes. This results in a maximum reliability performance of the secondary-side diodes in the designed converter, since the transition probability from operating state 1 (i.e., the healthy state) to operating state 3 (i.e., OC fault on the secondary-side diodes) is low. On the other hand, the OC fault on the primary-side switches has higher occurrence probability than on the diodes [i.e., $P_2(t) > P_3(t)$], which is even higher than that for the healthy operating state $[P_1(t)]$ in lower D and higher t values in the DCM operation mode. One can also observe, in Fig. 6, the unit probability of $P_1(t)$ and zero probability of $P_2(t)$ and $P_3(t)$ when $t = 0$, which indicate the initial condition in (5).

In order to investigate the reliability of IMSDC-DC converters as D changes, Fig. 7 depicts the reliability performance at $t = 0.3 \times 10^6$ and 0.6×10^6 h. The PP converter is concluded to have the highest reliability performance under different values of D. Although the voltage stress on the primary-side switches of this converter is twice that of the FB and HB converters, PP is characterized with less number of switches and capacitors than FB and HB converters. The additional components in the primary-side of the FB and HB converters, e.g., S_1 and S_4 switches, operate in series, which, in turn, degrades the reliability of FB and HB converters lower than that in PP converter. Moreover, the voltage gain of an HB converter is half of that in the PP converter, resulting in higher input voltage requirements and consequently higher stresses on the components to satisfy the same output power. In other words, considering all effective parameters on the reliability of these three IMSDC-DC converters, PP is attributed to a higher reliability performance under different D values. In order to evaluate the effect of the operating duty cycle on the reliability of IMSDC-DC converters, Fig. 8 illustrates the sensitivity of the system reliability with respect to D. The sensitivities are calculated through $[dR(D)/dD).(D/R(D))]$ in $t = 0.6 \times 10^6$ h. As shown in Fig. 8, the reliability of IMSDC-DC converters is more sensitive to the D variations under DCM

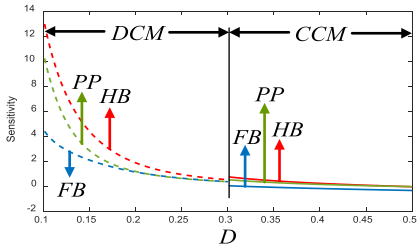

Fig. 8. Reliability sensitivity of IMSDC-DC converters with respect to duty cycle at $t = 0.6 \times 10^6$ h.

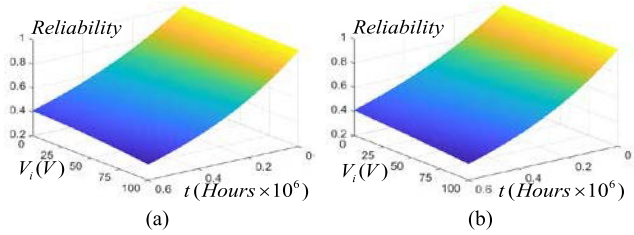

Fig. 9. Reliability with respect to input voltage and time duration. (a) DCM FB. (b) CCM FB.

operation mode than the CCM, which can be observed from Fig. 5(a) and (b), too. Moreover, the evaluated sensitivities are positive for the converters except for the FB in the CCM mode of operation, representing a degraded reliability in this operation mode.

B. Input Voltage

In some power electronic devices, e.g., photovoltaic power conditioning systems, the input voltage is variant over time. Therefore, a reliable converter design in its optimal range of input voltages is critical to ensure an acceptable operation continuously. In this section, the effect of variations in the input voltage V_i on the reliability of the IMSDC-DC converters is evaluated. Considering V_i variations, the components failure rates in a CCM HB converter for the healthy state are evaluated as follows:

$$\lambda_S(V_i) = 0.48 \exp\left(-1925\left(\frac{1}{298 + 2.18 \times 10^{-4} V_i^2 + 4.47 \times 10^{-2} V_i} - \frac{1}{298}\right)\right) \tag{13}$$

$$\lambda_D(V_i) = 2.052 \times 10^{-4} \exp\left(-3091\left(\frac{1}{298 + 6.75 \times 10^{-6} V_i^2 + 0.19 V_i} - \frac{1}{298}\right)\right) \tag{14}$$

$$\lambda_T(V_i) = 0.049 \exp\left(-1276\left(\frac{1}{298 + 1.978 \times 10^{-4} V_i^2} - \frac{1}{298}\right)\right) \tag{15}$$

$$\lambda_C(V_i) = 7.63 \times 10^{-3}\left(1.89 \times 10^{-8} V_i^3 + 1\right) \tag{16}$$

$$\lambda_{Co}(V_i) = 7.63 \times 10^{-3}\left(2.96 \times 10^{-7} V_i^3 + 1\right). \tag{17}$$

In Fig. 9, three-dimensional reliability plots of the DCM and CCM FB converters are demonstrated with respect to V_i and t. According to Fig. 9, DCM and CCM operation modes of an FB converter reveals an almost similar reliability characteristic as V_i changes. Note that V_i increase results in an inverse impact on the converter's overall reliability performance as the components stresses and power losses increase as well. Within the same lines, reliability of a DCM FB converter decreases from 0.4010 in $V_i = 25$ V to 0.3324 in $V_i = 100$ V at $t = 0.6 \times 10^6$, while the system reliability decreases from 0.3949 to 0.3359 in case of a CCM FB converter. In addition, the evaluated probability of the three operating states in a CCM FB converter is illustrated in

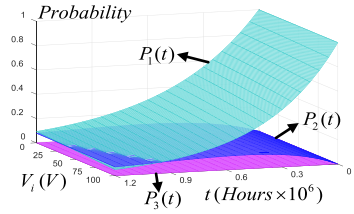

Fig. 10. Probability of operating states in CCM FB converter with respect to input voltage and time duration.

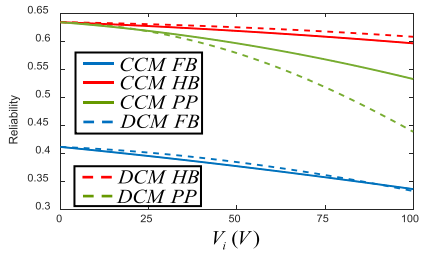

Fig. 11. Reliability comparison of CCM and DCM IMSDC-DC converters with respect to duty cycle at $t = 0.6 \times 10^6$ h.

Fig. 10, matching the observations in Fig. 9(b): the inequality of $P_1(t) > P_2(t) \gg P_3(t)$ is accurate for $t \leq 0.94 \times 10^6$ h given the specified range of V_i variations, reflecting the higher and lower probabilities of the healthy and diode OC fault operating states, respectively. In other words, the probability of the derated operating state with partial power operation is higher than that in the healthy operating state at $t > 0.94 \times 10^6$, particularly in higher values of V_i.

In Fig. 11, reliability performance of the IMSDC-DC converters are compared in a specific time duration, where DCM HB and CCM FB are attributed the highest and the lowest reliability performances, respectively. Sensitivities of the converters' reliability with respect to the input voltage and time duration variations are depicted in Fig. 12(a). The evaluated sensitivities in all IMSDC-DC converters are negative, reflecting (i) a reliability degradation of the IMSDC-DC converters due to V_i increments and (ii) the least sensitivity of the HB converter to the V_i variations. Moreover, the components' sensitivities are shown in Fig. 12(b) and (c) for DCM and CCM operations, respectively, where (i) the components of PP converter are the most sensitive and (ii) the evaluated results of Fig. 12(a) are verified.

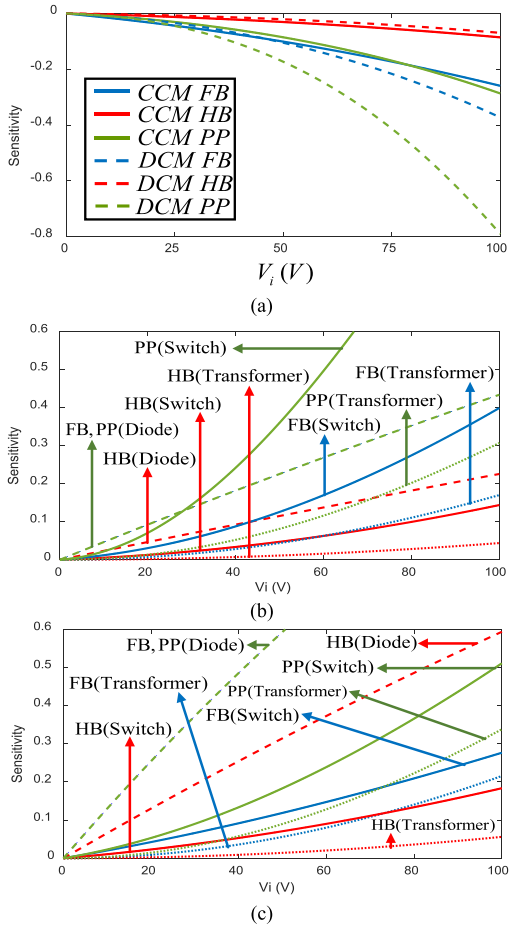

Fig. 12. Sensitivity comparison results of the IMSDC-DC with respect to the input voltage variations at $t = 0.6 \times 10^6$ h. (a) Overall sensitivities of the converters. (b) Components sensitivities in DCM. (c) Components sensitivities in DCM.

C. Output Power

A power electronic converter has to feed the output load under acceptable power or voltage conditions, and it contributes to its overall reliability performance over time. This section investigates the effect of P_o in various time durations on the converters' overall reliability performance. Based on the developed Markov models in Fig. 3(b), the component's failure rates in a CCM HB converter are evaluated using (1)–(6)

$$\lambda_S(P_o) = 0.48 \exp\left(-1925\left(\frac{1}{298 + 0.197P_o + 1.343\sqrt{P_o}} - \frac{1}{298}\right)\right) \tag{18}$$

$$\lambda_D(P_o) = 0.0038 \times \left(\frac{\sqrt{P_o}}{20}\right)^{2.43} \exp\left(-3091\left(\frac{1}{298 + 6.08 \times 10^{-3}P_o + 5.76\sqrt{P_o}} - \frac{1}{298}\right)\right) \tag{19}$$

$$\lambda_T(P_o) = 0.049 \exp\left(-1276\left(\frac{1}{298 + 0.178P_o} - \frac{1}{298}\right)\right) \tag{20}$$

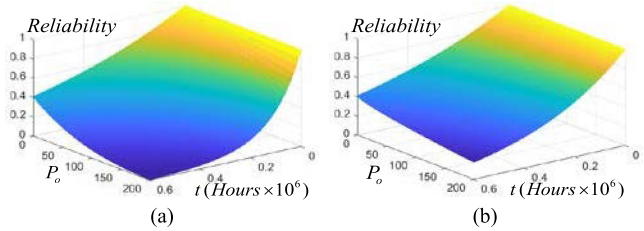

Fig. 13. Reliability performance with respect to variations in output power and time duration. (a) DCM FB. (b) CCM FB.

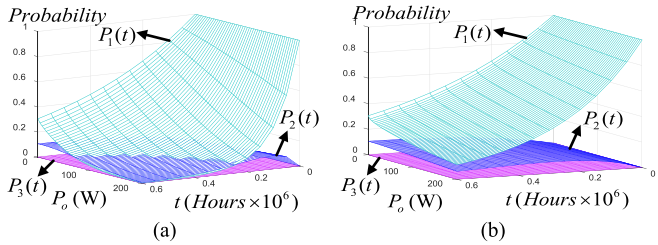

Fig. 14. Probability of operating states with respect to variations in output voltage and time duration. (a) DCM FB. (b) CCM FB.

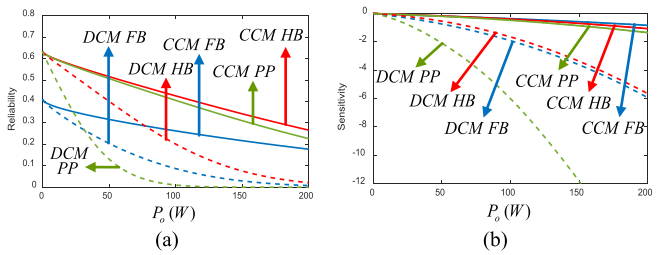

Fig. 15. Comparison of the IMSDC-DC converters with respect to the output power in CCM and DCM operation modes in $t = 0.6 \times 10^6$ h. (a) Reliability. (b) Reliability sensitivity.

$$\lambda_C(P_o) = 7.63 \times 10^{-3}\left(8 \times 10^{-3}P_o^{1.5} + 1\right) \tag{21}$$

$$\lambda_{Co}(P_o) = 7.63 \times 10^{-3}\left(5.12 \times 10^{-4}P_o^{1.5} + 1\right). \tag{22}$$

Three-dimensional reliability plots of the DCM and CCM FB converter in this test case are demonstrated in Fig. 13(a) and (b). The impact of P_o variations on the converter's reliability is observed having a similar trend to that in the previous test case with V_i variations, but with different rates. One can see that the operation of the DCM FB converter in $t > 0.3 \times 10^6$ h and $P_o > 100$ W is not optimal under this particular design, while the CCM FB converter still offers a better operational condition under the same P_o and t regions. This nonoptimal region for FB DCM operation is verified in Fig. 14(a), where $P_1(t)$ has a very low probability—even lower than $P_2(t)$. The probabilities corresponding to the operating states of the DCM FB converter in $t = 0.3 \times 10^6$ and $P_o = 100$ W are found to be $P_1(t) = 0.1861$, $P_2(t) = 0.1028$, and $P_3(t) = 0.00004$, while the corresponding values for a CCM FB are assessed equal to 0.4180, 0.0963, and 0.0004, respectively [see Fig. 14(b)].

In Fig. 15, the reliability performance of the IMSDC-DC converters and its sensitivity are compared under different P_o scenarios and fixed time duration of $t = 0.6 \times 10^6$ h. Fig. 15(a) illustrates the reliability performance of the aforementioned converters in both DCM and CCM operation modes, where CCM operation of each converter is attributed a higher reliability than that in the DCM operation mode. This observation verifies the conclusions made from Fig. 7, where the DCM operation requires a higher input power to satisfy the specific output load power requirements. Moreover, the FB converter is found to be less reliable than others due to its more switches. In Fig. 15(b), the reliability sensitivity of the converters is presented, where their negative values validate the inverse impact of P_o increments on the converters' reliability performance. Furthermore, the CCM operation is found more robust against P_o changes from a reliability point of view.

D. Transformer Turns Ratio

Selection of higher transformer turns ratios in designing the isolated power electronic converters results in higher output voltage levels, which, in turn, imposes higher current stress on the primary-side semiconductors. A tradeoff, hence, is needed to determine its optimal region. In this article, the transformer turns ratio is defined as $n : 1$, with respect to which, the first state components failure rates in a CCM HB converter are expressed as follows:

$$\lambda_S(n) = 0.48 \exp\left(-1925\left(\frac{1}{298 + 19.047n^2 + \frac{0.663}{n^2} + \frac{13.553}{n}} - \frac{1}{298}\right)\right) \tag{23}$$

$$\lambda_D(n) = 3.837 \times 10^{-3} \tag{24}$$

$$\lambda_T(n) = 0.049 \exp\left(-1276\left(\frac{1}{304.82 + \frac{10.989}{n^2}} - \frac{1}{298}\right)\right) \tag{25}$$

$$\lambda_C(n) = 7.63 \times 10^{-3}\left(8n^3 + 1\right) \tag{26}$$

$$\lambda_{Co}(n) = 1.154 \times 10^{-2} \tag{27}$$

where power loss and failure rates of the secondary-side diodes (λ_D) and output capacitor (λ_{Co}) are almost independent of n [23]. In Fig. 16, reliability of the DCM and CCM PP converter are illustrated with respect to the transformer turns ratio n and time duration t, where it can be found that the CCM operation is more reliable than DCM, particularly for $0.3 \leq n \leq 2.5$. Moreover, the converter's reliability performance reaches a maximum in both DCM and CCM operation modes. The probability of each operating state is presented in Fig. 17, where one can see that $P_2(t)$ decreases in higher values of n —this is due to lower current stress and power loss on the primary-side switches when n increases given the condition that the output power remains constant. In other words, the OC fault incidence on the primary-side switches is less probable in higher values of n. In Fig. 18, the reliability performance and its sensitivity

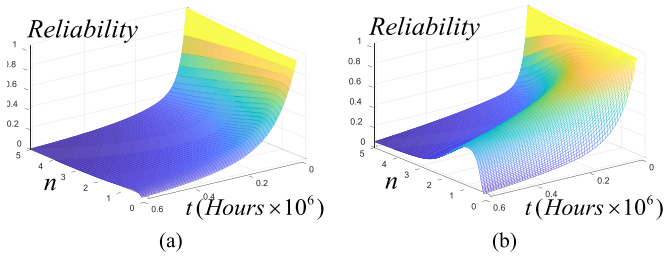

Fig. 16. Reliability with respect to transformer turns ratio and time duration. (a) DCM PP. (b) CCM PP.

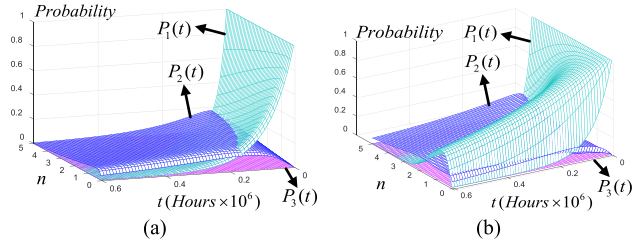

Fig. 17. Probability of operating states with respect to transformer turns ratio and time duration. (a) DCM PP. (b) CCM PP.

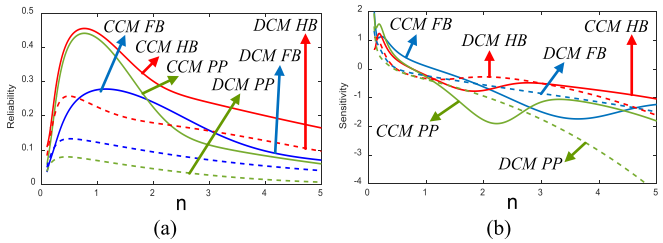

Fig. 18. Comparison of the IMSDC-DC converters with respect to transformer turns ratio in $t = 0.6 \times 10^6$ h under CCM and DCM operation modes. (a) Reliability. (b) Reliability sensitivity.

comparisons are presented among different IMSDC-DC converters. According to Fig. 18(a), reliability of the FB, HB, and PP converters reaches a maximum value in $n = 1.14, 0.77$, and 0.76 under CCM operation mode, respectively, while they are 0.51, 0.49, and 0.45 under DCM operation modes. In order to better demonstrate the impact of n on the reliability performance of the converters, Fig. 18(b) compares its sensitivities in IMSDC-DC converters with respect to n. Both positive and negative values confirm the direct and inverse effect of n on the reliability values, respectively. Note that the zero sensitivity values in Fig. 18(b) reflect the maximum reliability points.

E. Voltage Gain

DC–DC power converters are primarily designed to change and regulate the input voltage to the output load voltage. In many industrial applications (e.g., different types of dc power supplies), both the input and output voltage levels of the converters could be constant or variant, as a result of which, the converter operates with a variable voltage gain. This section focuses on the optimal reliability region of the IMSDC-DC converters

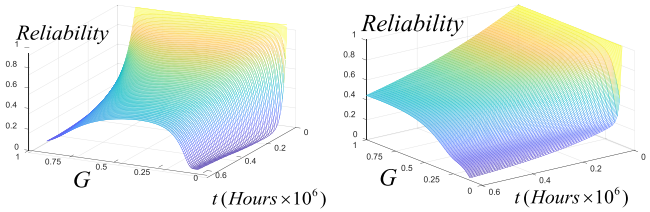

Fig. 19. Reliability with respect to voltage gain and time duration. (a) DCM PP. (b) CCM PP.

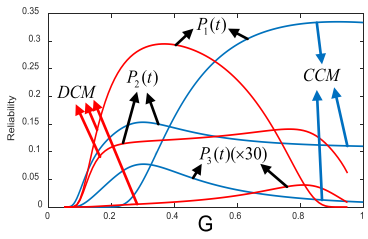

Fig. 20. Probability of operating states with respect to voltage gain in PP converter in $t = 0.6 \times 10^6$ h under DCM and CCM operation modes.

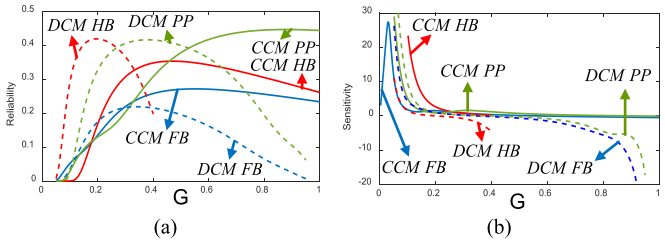

Fig. 21. Comparison of IMSDC-DC converters with respect to voltage gain in $t = 0.6 \times 10^6$ h under CCM and DCM operation modes. (a) Reliability. (b) Reliability sensitivity.

in their buck operation. According to the voltage gain equations of the FB, HB, and PP converters, i.e., $G = 2D/n$, D/n, and $2D/n$ for CCM operation mode and $G = D/n(D + D_1)$, $D/2n(D + D_1)$, and $D/n(D + D_1)$ for DCM operation mode, respectively, the effect of G on the IMSDC-DC converters is characterized through D and n. In the preceding DCM equations, D_1 indicates the interval when all primary-side switches and secondary-side diodes are OFF and ON, respectively.

Fig. 19(a) and (b), respectively, illustrate the reliability performance of the PP converter versus G and t variations under DCM and CCM operation modes. $G = 0.53$ is found to be the boundary where the converter reliability under each DCM and CCM operations is higher on one side of the curves, representing the corresponding operating conditions. This boundary is equal to $G = 0.29$ and 0.33 for the FB and HB converters, respectively. The probability of the PP converter's operating states is depicted in Fig. 20, where $P_1(t) > P_2(t)$ is valid for higher G values under CCM operation modes, while the reverse would be effective under DCM operation modes. In Fig. 21, the reliability performance and its sensitivity are presented for the IMSDC-DC converters. According to Fig. 21(a), one G value is found for each converter in which a maximum reliability performance is achieved. The maximum reliability points for the FB, HB, and PP converters are assessed when $G = 0.55$, 0.47, and 0.88 under CCM and 0.34, 0.20, and 0.38 under DCM operation modes, respectively. As observed in Fig. 21(b), the IMSDC-DC converters reliability performance is more robust against G variations within the $0.3 < G < 0.6$ region, while the sensitivities are high when $G < 0.2$ for both DCM and CCM operation modes and in $0.8 < G < 1$ for DCM operation mode.

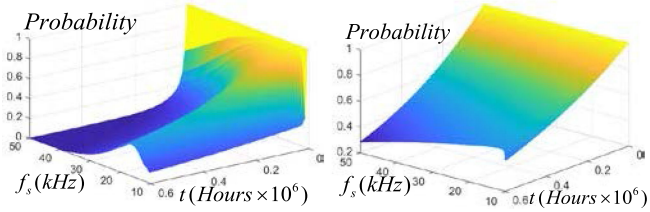

Fig. 22. Reliability with respect to switching frequency and time duration. (a) DCM PP. (b) CCM PP.

F. Switching Frequency

A design degree of freedom in modern power electronic converters is typically characterized through the switching frequency, which affects the value and size of the passive components, semiconductor selections, and the operating point of transformer according to its saturation curve. This section investigates the impact of f_s on the reliability performance of IMSDC-DC converters. Considering a fixed set of components, the first state components failure rates in a CCM HB converter are given as

$$\lambda_S(f_s) = 0.48 \exp\left(-1925\left(\frac{1}{312.204+9.52\times10^{-4}f_s} - \frac{1}{298}\right)\right) \tag{28}$$

$$\lambda_D(f_s) = 3.837 \times 10^{-3} \tag{29}$$

$$\lambda_T(f_s) = 6.238 \times 10^{-2} \tag{30}$$

$$\lambda_C(f_s) = 6.87 \times 10^{-2} \tag{31}$$

$$\lambda_{Co}(f_s) = 1.154 \times 10^{-2} \tag{32}$$

where $\lambda_S(f_s)$—the failure rate of the primary-side switches—is the only f_s-dependent parameter due to its switching loss [23]. In Fig. 22, reliability of PP converter is expressed as a function of f_s and t, according to which, both DCM and CCM operation modes are attributed a maximum reliability performance directly driven by the initial design and semiconductor selections. In other words, passive components are selected with higher values to achieve the same ripple characteristics in lower f_s values, which, in turn, increases the power loss. In addition, the switching loss in the primary-side switches increases the failure rates in higher values of f_s and, hence, the converter reliability is found to have a peak value. Fig. 23 demonstrates the partial probability of each operating state for the PP converter. Under a DCM operation mode, $P_1(t) > P_2(t)$ is valid only within a narrow region of

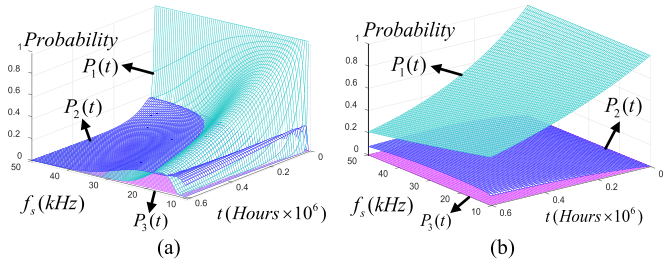

Fig. 23. Probability of operating states with respect to switching frequency and time duration. (a) DCM PP. (b) CCM PP.

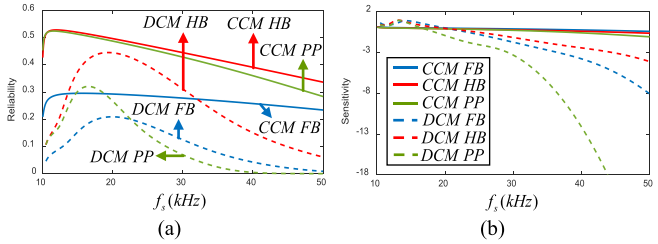

Fig. 24. Comparison of IMSDC-DC converters with respect to switching frequency in $t = 0.6 \times 10^6$ h under CCM and DCM operation modes. (a) Reliability. (b) Reliability sensitivity.

14 kHz $< f_s <$ 20 kHz in the specified time duration, which verifies a high power loss and failure probability of the primary-side switches in higher switching frequency. In Fig. 24(a) and (b), the reliability performance and its sensitivity with respect to f_s are demonstrated, respectively. The FB converter is found less reliable owing to the additional number of primary-side switches resulting in higher switching losses. Furthermore, the reliability of the DCM PP reaches its minimum in higher values of f_s, since higher energy is lost in each switching transition with switch voltage stress of $2\,V_i$. In Fig. 24(a), the reliability performance of the FB, HB, and PP converters reach the maximum values in $f_s = 16.1$, 12.1, and 11.7 kHz for CCM and 19.9, 19.3, and 16.6 kHz for DCM operation modes, respectively. From the results presented in Fig. 24(b), one can see that the reliability in the CCM operation mode is generally more robust, while the DCM PP is affected the most with f_s variations.

G. Components' Characteristics

Component characteristics in power electronic converters affect the power losses and subsequently the failure rate values. As concluded earlier, switches are found to have the most effective failure rate factor among other components in the IMSDC-DC converters. Hence, the impact of switch characteristics on its failure rate is assessed. For demonstration purposes, several sample switches with different characteristics are selected from the same family (i.e., IRFP4xxxPbF power MOSFETs) and their effective factors on λ_S are tabulated in Table I. The contributing factors are the drain-source breakdown voltage $(V_{\rm DS})$, drain-source ON-resistance $(R_{\rm DS})$, output capacitance $(C_{\rm oss})$, and turn-on and -off delay times $(T_{d(\rm on)}$ and $T_{d(\rm off)})$. The λ_S factors of the IMSDC-DC converters are then evaluated according to

TABLE I
IMPORTANT CHARACTERISTICS OF SELECTED POWER SWITCHES ON IMSDC-DC CONVERTER RELIABILITY

Parameters	IRFPxxxxPbF Power MOSFETs					
	4242	4232	4229	4137	4668	4868
$V_{\rm DS}$ (V)	360	300	300	300	200	300
$R_{\rm DS}$ (mΩ)	49	30	38	56	8	25.5
$C_{\rm oss}$ (pF)	520	610	390	300	810	612
$T_{d(\rm on)}$ (nS)	40	37	25	18	41	24
$T_{d(\rm off)}$ (nS)	72	64	44	34	64	62

TABLE II
CALCULATED FAILURE RATES OF SELECTED POWER SWITCHES UNDER DCM OPERATION MODE

	Converters	IRFPxxxxPbF Power MOSFETs					
		4242	4232	4229	4137	4668	4868
State 1	FB	1.378	1.550	1.200	1.052	2.056	1.613
	HB	1.610	1.845	1.360	1.163	2.524	1.915
	PP	6.480	8.211	4.468	3.204	12.836	8.370
State 2	FB	0.825	0.888	0.755	0.698	1.055	0.904
	HB	0.907	0.989	0.813	0.740	1.206	1.006
	PP	2.396	2.907	1.795	1.412	4.269	2.941

TABLE III
CALCULATED FAILURE RATES OF SELECTED POWER SWITCHES UNDER CCM OPERATION MODE

	Converters	IRFPxxxxPbF Power MOSFETs					
		4242	4232	4229	4137	4668	4868
State 1	FB	0.706	0.714	0.746	0.737	0.792	0.769
	HB	0.918	0.968	0.908	0.859	1.163	1.036
	PP	0.918	0.968	0.908	0.859	1.163	1.036
State 2	FB	0.644	0.660	0.648	0.632	0.722	0.686
	HB	0.684	0.707	0.678	0.655	0.789	0.734
	PP	0.962	1.049	0.882	0.805	1.294	1.085

the components' operational characteristics and initial design assumptions. Tables II and III present the evaluated λ_S for different switches under DCM and CCM operation modes, respectively, where (i) the contribution of each factor on the failure rates is quantified, and (ii) it can be found that the type of the converter along with all the other parameters contribute to the λ_S results. Comparison of the results presented in Tables II and III demonstrates higher λ_S values under DCM operation mode than the CCM mode, resulting in a lower reliability performance of DCM in IMSDC-DC converters.

V. MTTF ANALYSIS OF IMSDC-DC CONVERTERS

This section quantifies and analyzes the MTTF index of reliability for the IMSDC-DC converters according to (7) and the results are presented in Fig. 25. The MTTF is presented with respect to variations in D, V_i, P_o, n, G, and f_s in Fig. 25(a)–(f), respectively. The MTTF overall follows the corresponding reliability performance metric analyzed earlier for each IMSDC-DC converter. The reason lies in the underlying independency of t to D, V_i, P_o, n, G, and f_s, where MTTF is calculated through integration of the reliability metrics with respect to t.

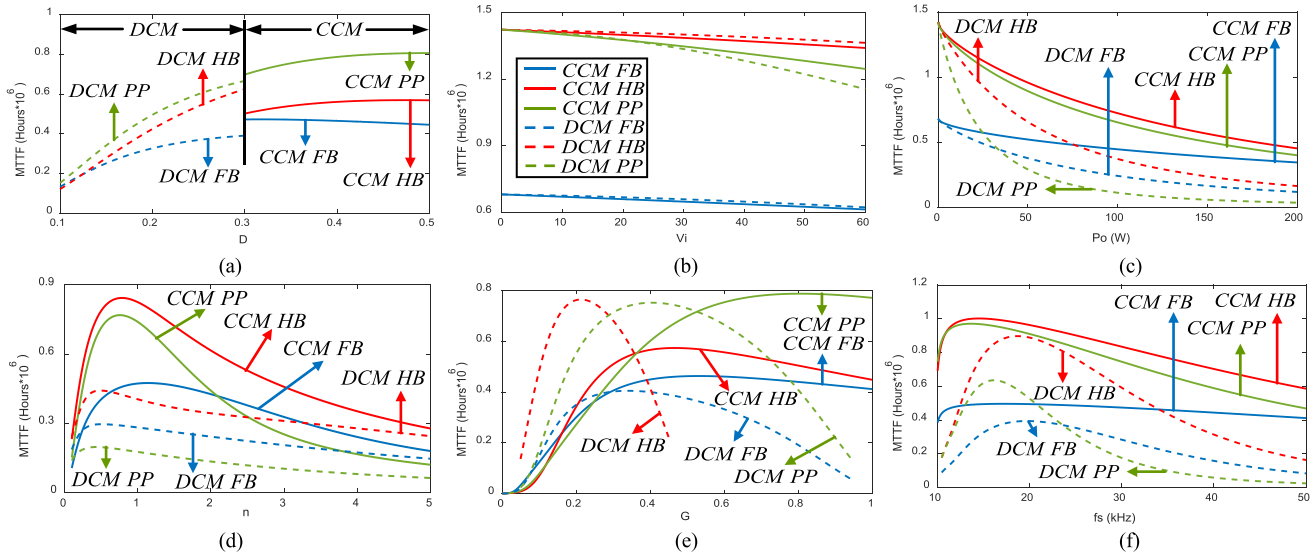

Fig. 25. MTTF comparison of the IMSDC-DC converters under CCM and DCM operation modes with respect to (a) duty cycle, (b) input voltage, (c) output power, (d) transformer turns ratio, (e) voltage gain, and (f) switching frequency.

Eventually, the extensive reliability analysis presented in this article offers the following optimal operation regions of the IMSDC-DC converters:

1) **DCM FB:** $0.2 < D < 0.3$, $0 < V_i < 50(\mathrm{V})$, $0 < P_o < 51(\mathrm{W})$, $0.2 < n < 1.8$, $0.24 < G < 0.48$, and $17.7 < f_s < 22.5$ (kHz)
2) **CCM FB:** $0.3 < D < 0.4$, $0 < V_i < 34(\mathrm{V})$, $0 < P_o < 171(\mathrm{W})$, $0.22 < n < 3.9$, $0.27 < G < 1$, and $10.5 < f_s < 35$ (kHz)
3) **DCM HB:** $0.16 < D < 0.3$, $0 < V_i < 196(\mathrm{V})$, $0 < P_o < 100(\mathrm{W})$, $0.11 < n < 4.9$, $0.08 < G < 0.4$, and $13.1 < f_s < 33$ (kHz)
4) **CCM HB:** $0.4 < D < 0.5$, $0 < V_i < 175(\mathrm{V})$, $0 < P_o < 250(\mathrm{W})$, $0.08 < n < 7$, $0.21 < G < 1$, and $9.6 < f_s < 64$ (kHz)
5) **DCM PP:** $0.13 < D < 0.3$, $0 < V_i < 62(\mathrm{V})$, $0 < P_o < 39(\mathrm{W})$, $0.38 < n < 0.95$, $0.14 < G < 0.8$, and $13.9 < f_s < 20.3$ (kHz)
6) **CCM PP:** $0.4 < D < 0.5$, $0 < V_i < 88(\mathrm{V})$, $0 < P_o < 218(\mathrm{W})$, $0.14 < n < 3.4$, $0.3 < G < 1$, and $9.2 < f_s < 53$ (kHz)

VI. Experimental Results: Verifications

This section is devoted to confirm the operation principles of Section II and the discussed self-embedded fault-tolerant capability of the IMSDC-DC converters through experimental verifications. The experimental tests are performed on the developed FB, HB, and PP prototypes, which are as follows:

1) SC and OC fault occurrences;
2) CCM and DCM operations;
3) different D, V_i, P_o, n, and G values;
4) various combinations of consecutive faults.

The results are presented in Fig. 26: (a) through (d) for FB converter, (e) through (h) for HB converter and (i), (j) for PP converter. As the general results of Fig. 26, the occurrence of an OC and an SC as the first faults in the primary- or secondary-side semiconductors lead to a de-rated and absorbing operating states, respectively. In addition, the behavior of the converters under the second OC fault depends on the category of failed components' combination, which is explained in Section II. As examples, in Fig. 26(a) and (b), two consecutive OC faults on two corresponding semiconductors result in de-rated operating states of the converter. In Fig. 26(c) and (d), two consecutive OC faults on two complementary semiconductors lead to an absorbing operating state [i.e., the OC fault on the switch S_1 is followed by a second OC fault on one of its complementary semiconductors-S_2 in Fig. 26(c) and D_2 in Fig. 26(d)]. In addition, SC fault of any component in all IMSDC-DC converters leads to the absorbing state in Fig. 26(f) and (j).

VII. Conclusion

This article focused on the comprehensive reliability evaluation of the IMSDC-DC power electronic converters. Numerical analytics was proposed to capture the effects of various prevailing factors, e.g., operation time duration, duty cycle, input voltage, output power, transformer turns ratio, voltage gain, switching frequency, and components characteristics, on the reliability performance of the converters over time. Both DCM and CCM modes of operations in the IMSDC-DC converters were assessed considering various scenarios including the OC and SC fault incidents on each component. The self-embedded fault-tolerant capability of the IMSDC-DC converters was extensively discussed under OC fault conditions on the switches, diodes, and blocking capacitors. Markov models of the converters were characterized based on the IMSDC-DC operation principles, centered on which the reliability performance and MTTF metrics were numerically evaluated and confirmed through a suite of experimental verifications. As a brief conclusion of the article,

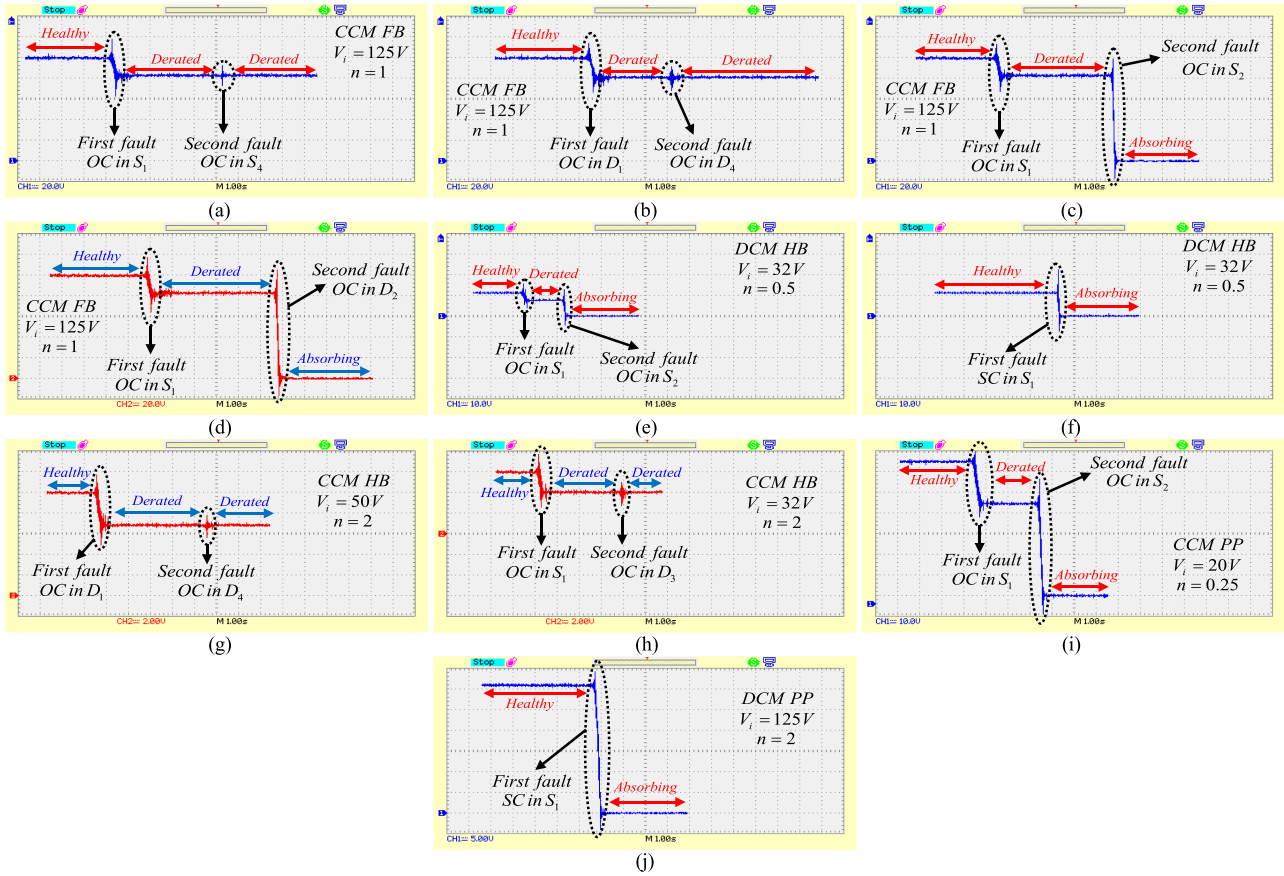

Fig. 26. Experimental output voltage waveform of the IMSDC-DC converters under different faults scenarios and operation characteristics.

increasing input voltage and output power have inverse relation with reliability value. However, there is an optimum point in the calculated reliability of each IMSDC-DC converter in terms of duty cycle, transformer turns ratio, voltage gain, and switching frequency. Moreover, CCM operation of IMSDC-DC converters is more reliable in most of the operational scenarios.

REFERENCES

[1] U. M. Choi, F. Blaabjerg, S. Jørgensen, S. Munk-Nielsen, and B. Rannestad, "Reliability improvement of power converters by means of condition monitoring of IGBT modules," *IEEE Trans. Power Electron.*, vol. 32, no. 10, pp. 7990–7997, Oct. 2017.

[2] H. Behjati and A. Davoudi, "Reliability analysis framework for structural redundancy in power semiconductors," *IEEE Trans. Ind. Electron.*, vol. 60, no. 10, pp. 4376–4386, Oct. 2013.

[3] D. Zhou, F. Blaabjerg, T. Franke, M. Tønnes, and M. Lau, "Comparison of wind power converter reliability with low-speed and medium-speed permanent-magnet synchronous generators," *IEEE Trans. Ind. Electron.*, vol. 62, no. 10, pp. 6575–6584, Oct. 2015.

[4] H. Tarzamni, F. Tahami, M. Fotuhi-Firuzabad, and F. P. Esmaeelnia, "Reliability analysis of buck-boost converter considering the effects of operational factors," in *Proc. 10th Int. Power Electron., Drive Syst. Technol. Conf*, 2019, pp. 647–652.

[5] S. Yang, A. Bryant, P. Mawby, D. Xiang, L. Ran, and P. Tavner, "An industry-based survey of reliability in power electronic converters," *IEEE Trans. Ind. Appl.*, vol. 47, no. 3, pp. 1441–1451, May/Jun. 2011.

[6] D. Zhou, H. Wang, and F. Blaabjerg, "Mission profile based system-level reliability analysis of DC/DC converters for a backup power application," *IEEE Trans. Power Electron.*, vol. 33, no. 9, pp. 8030–8039, Sep. 2018.

[7] M. K. Alam and F. H. Khan, "Reliability analysis and performance degradation of a boost converter," *IEEE Trans. Ind. Appl.*, vol. 50, no. 6, pp. 3986–3994, Nov./Dec. 2014.

[8] Y. Liu, M. Huang, H. Wang, X. Zha, J. Gong, and J. Sun, "Reliability-oriented optimization of the LC filter in a buck DC-DC converter," *IEEE Trans. Power Electron.*, vol. 32, no. 8, pp. 6323–6337, Aug. 2017.

[9] T. Rahimi, S. H. Hosseini, M. Sabahi, M. Abapour, and G. B. Gharehpetian, "Three-phase soft-switching-based interleaved boost converter with high reliability," *IET Power Electron.*, vol. 10, no. 3, pp. 377–386, Mar. 2017.

[10] Y. C. Hsieh, T. C. Hsueh, and H. C. Yen, "An interleaved boost converter with zero-voltage transition," *IEEE Trans. Power Electron.*, vol. 24, no. 4, pp. 973–978, Apr. 2009.

[11] N. Jain, P. K. Jain, and G. Joos, "A zero voltage transition boost converter employing a soft switching auxiliary circuit with reduced conduction losses," *IEEE Trans. Power Electron.*, vol. 19, no. 1, pp. 130–139, Jan. 2004.

[12] F. H. Aghdam and M. Abapour, "Reliability and cost analysis of multistage boost converters connected to PV panels," *IEEE J. Photovol.*, vol. 6, no. 4, pp. 981–989, Jul. 2016.

[13] A. Khosroshahi, M. Abapour, and M. Sabahi, "Reliability evaluation of conventional and interleaved DC–DC boost converters," *IEEE Tran. Power Electron.*, vol. 30, no. 10, pp. 5821–5828, Oct. 2015.

[14] S. V. Dhople, A. Davoudi, A. D. Domínguez-García, and P. L. Chapman, "A unified approach to reliability assessment of multiphase DC–DC converters in photovoltaic energy conversion systems," *IEEE Trans. Power Electron.*, vol. 27, no. 2, pp. 739–751, Feb. 2012.

[15] H. Tarzamni, E. Babaei, A. Zarrin Gharehkoushan, and M. Sabahi, "Interleaved full ZVZCS DC–DC boost converter: Analysis, design, reliability evaluations and experimental results," *IET Power Electron.*, vol. 10, no. 7, pp. 835–845, Jun. 2017.

[16] X. Pei, S. Nie, Y. Chen, and Y. Kang, "Open-circuit fault diagnosis and fault-tolerant strategies for full-bridge DC–DC converters," *IEEE Trans. Power Electron.*, vol. 27, no. 5, pp. 2550–2565, May 2012.

[17] Z. Gao, C. Cecati, and S. X. Ding, "A survey of fault diagnosis and fault-tolerant techniques-part I: Fault diagnosis with model-based and signal- based approaches," *IEEE Trans. Ind. Electron.*, vol. 62, no. 6, pp. 3757–3767, Jun. 2015.
[18] Z. Gao, C. Cecati, and S. X. Ding, "A survey of fault diagnosis and fault-tolerant techniques-part II: Fault diagnosis with knowledge-based and hybrid/active approaches," *IEEE Trans. Ind. Electron.*, vol. 62, no. 6, pp. 3768–3774, Jun. 2015.
[19] H. Khoun Jahan, F. Panahandeh, M. Abapour, and S. Tohidi, "Reconfigurable multilevel inverter with fault tolerant ability," *IEEE Trans. Power Electron.*, vol. 33, no. 9, pp. 7880–7893, Sep. 2018.
[20] M. M. Haji-Esmaeili, M. Naseri, H. Khoun-Jahan, and M. Abapour, "Fault tolerant structure for cascaded h-bridge multi-level inverter and reliability evaluation," *IET Power Electron.*, vol. 10, no. 1, pp. 59–70, Jan. 2017.
[21] B. Mirafzal, "Survey of fault-tolerance techniques for three-phase voltage source inverters," *IEEE Trans. Ind. Electron.*, vol. 61, no. 10, pp. 5192–5202, Oct. 2014.
[22] S. Kim, J. Lee, and K. Lee, "A modified level-shifted PWM strategy for fault-tolerant cascaded multilevel inverters with improved power distribution," *IEEE Trans. Ind. Electron.*, vol. 63, no. 11, pp. 7264–7274, Nov. 2016.
[23] M. K. Kazimierczuk, *Pulse-Width Modulated DC-DC Power Converters*. New York, NY, USA: Wiley, 2008, pp. 139–188.
[24] R. Billinton and R. N. Allan, *Reliability Evaluation of Engineering Systems, Concepts and Techniques*. 2nd ed.. New York, NY, USA: Springer-Verlag, 1992, pp. 260–306.
[25] R. Wu, F. Blaabjerg, H. Wang, M. Liserre, and F. Iannuzzo, "Catastrophic failure and fault-tolerant design of IGBT power electronic converters—An overview," in *Proc. 39th Annu. Conf. IEEE Ind. Electron. Soc.*, 2013, pp. 507–513.
[26] "Reliability prediction of electronic equipments," Relex Software Corp., Greensburg, PA, USA, Rep. MIL-HDBK-217, 1990.
[27] "Reliability prediction models," Reliability Information Analysis Center, RIAC-MIL-HDBK-217Plus, 2006.

Hadi Tarzamni (S'18) was born in Tabriz, Iran, in 1992. He received the B.Sc. and M.Sc. degrees with first class honors in power electrical engineering from the Faculty of Electrical and Computer Engineering, University of Tabriz, Tabriz, Iran, in 2014 and 2016, respectively. He is currently working toward the Ph.D. degree in power electronics engineering with the Department of Electrical Engineering, Sharif University of Technology, Tehran, Iran.

He has authored and coauthored 15 journals and conference papers. He also holds six patents in the area of power electronics. His research interests include power electronic converters analysis and design, dc–dc converters, soft-switching and resonant converters, and reliability analysis.

Farhad Panahandeh Esmaeelnia was born in Tabriz, Iran, in 1993. He received the B.Sc. and M.Sc. degrees in power electrical engineering from the Faculty of Electrical and Computer Engineering, University of Tabriz, Tabriz, Iran, in 2015 and 2017, respectively.

His research interests include reliability of power electronics, power electronic converters analysis and design, renewable energy, photovoltaic systems, demand response, and energy management.

Mahmud Fotuhi-Firuzabad (F'14) received the B.Sc. and M.Sc. degrees in electrical engineering from the Sharif University of Technology and Tehran University, Tehran, Iran, in 1986 and 1989, respectively, and the M.Sc. and Ph.D. degrees in electrical engineering from the University of Saskatchewan, Saskatoon, SK, Canada, in 1993 and 1997, respectively.

He is a Professor with Electrical Engineering Department and President with the Sharif University of Technology. He is a member of Center of Excellence in Power System Control and Management in the same department. He is a Visiting Professor with Aalto University, Espoo, Finland. His research interests include power system reliability, distributed renewable generation, demand response, and smart grids.

Dr. Fotuhi-Firuzabad is the recipient of several national and international awards including World Intellectual Property Organization Award for the Outstanding Inventor, 2003, and PMAPS International Society Merit Award for contributions of probabilistic methods applied to power systems in 2016. He serves as the Editor-In-Chief of the IEEE POWER ENGINEERING LETTERS and also the Editor of *Journal of Modern Power Systems and Clean Energy*.

Farzad Tahami (M'97–SM'12) received the B.S. degree in electrical engineering from the Ferdowsi University of Mashhad, Mashhad, Iran, in 1991, and the M.S. and Ph.D. degrees in electrical engineering from the University of Tehran, Tehran, Iran, in 1993 and 2003, respectively.

From 1991 to 2004, he was with R&D Department, Jovain Electrical Machines Corporation, Iran. In 2004, he joined the Sharif University of Technology, Tehran, Iran, where he is currently an Associate Professor. Since 2007, he has been the Chairman of the Technical Committee of Rotating Machinery, The Iranian National Electrotechnical Committee. His current research interests include electric motor drives, modeling and control of power electronic converters, soft switching, resonant converters, high-frequency power conversion, and wireless power transfer.

Dr. Tahami is a member of the Board of Directors and the Chairman of the Education Committee of the Power Electronics Society of Iran.

Sajjad Tohidi was born in Meshkin Shahr, Iran, in 1984. He received the B.Sc. degree from the Iran University of Science and Technology, Tehran, Iran, in 2006, and the M.Sc. and Ph.D. degrees from the Sharif University of Technology, Tehran, Iran, in 2008, and 2012, respectively.

He is currently an Associate Professor with the Faculty of Electrical and Computer Engineering, University of Tabriz, Tabriz, Iran. His research interests include power systems dynamics, electrical machines, and wind power generation.

Payman Dehghanian (S'11–M'17) received the B.Sc. degree from the University of Tehran, Tehran, Iran, in 2009, the M.Sc. degree from the Sharif University of Technology, Tehran, Iran, in 2011, and the Ph.D. degree from Texas A&M University, College Station, TX, USA, in 2017, all in electrical engineering.

He is an Assistant Professor with the Department of Electrical and Computer Engineering, George Washington University, Washington, DC, USA. His research interests include power system protection and control, power system reliability and resiliency, asset management, and smart electricity grid applications.

Dr. Dehghanian is the recipient of the 2013 IEEE Iran Section Best M.Sc. Thesis Award in electrical engineering, the 2014 and 2015 IEEE region 5 outstanding professional achievement awards, and the 2015 IEEE-HKN Outstanding Young Professional Award.